INTERNATIONAL JOURNAL FOR NUMERICAL METHODS IN FLUIDS, VOL. 24, 595–613 (1997)

SOLUTION OF THE ADVECTION–DIFFUSION EQUATION USING A COMBINATION OF DISCONTINUOUS AND MIXED FINITE ELEMENTS

P. SIEGEL, R. MOSÉ AND PH. ACKERER

Institut de Mécanique des Fluides, Université Louis Pasteur, URA CNRS 854, 2 Rue Boussingault, F-67000 Strasbourg, France

AND

J. JAFFRE

Institut de Recherche en Informatique et Automatique, Domaine de Voluceau, Rocquencourt, F-78153 Le Chesnay Cedex, France

SUMMARY

When transport is advection-dominated, classical numerical methods introduce excessive artificial diffusion and spurious oscillations. Special methods are required to overcome these phenomena. To solve the advection–diffusion equation, a numerical method is developed using a discontinuous finite element method for the discretization of the advective terms. At the discontinuities of the approximate solution, numerical advective fluxes are calculated using one-dimensional approximate Riemann solvers. The method is stabilized with a multidimensional slope limiter which introduces small amounts of numerical diffusion when sharp concentration fronts occur. In addition, the diffusive term is discretized using a mixed hybrid finite element method. With this approach, numerical oscillations are completely avoided for a full range of cell Peclet numbers. The combination of discontinuous and mixed finite elements can be easily applied to 2D and 3D models using various types of elements in regular and irregular meshes. Numerical tests show good agreement with 1D and 2D analytical solutions. This approach is compared at the same time with two different numerical methods, a standard mixed finite method and a finite volume approach with high-resolution upwind terms. Regular and irregular meshes are used for the numerical tests to study the mesh effects on the numerical results. Our data show that in all cases this approach performs well. © 1997 by John Wiley & Sons, Ltd.

KEY WORDS: advection–diffusion equation; discontinuous finite element method; mixed finite element method; solute transport in porous media

INTRODUCTION

Finite elements and finite differences are classical methods used to solve the advection–diffusion equation. This equation depends on the relative importance of the advective and diffusive fluxes on the level of an element. When the transport is advection-dominated, the equation becomes hyperbolic. The resolution of this equation by classical methods introduces excessive artificial diffusion and spurious oscillations.[1] Both these problems disappear if one refines the space and time grids. However, in practice this cannot be done because of the considerable increase in computational effort.

CCC 0271–2091/97/060595–19 $17.50

Received 29 March 1995
Revised 17 July 1996

Alternative methods have been developed to solve the advection–diffusion equation without these phenomena of numerical diffusion and oscillations.

Two approaches are possible: one is based on the characteristic method or called the Eulerian–Lagrangian method, which was introduced in the 1950s, and the other is based on a Eulerian approach.

Characteristic methods decouple advection from diffusion in the transport equation. Many approaches have been developed based on this concept: the method of characteristics[2,3] and the modified method of characteristics[4] are the most popular examples of the application of this concept. In these approaches there is no restriction on the Courant number, which was the greatest interest of these methods. Other classes of Eulerian–Lagrangian methods have been developed in the 1980s and 1990s in conjunction with weak formulations such as the Galerkin Eulerian–Lagrangian formulation[5] and the Eulerian–Lagrangian localized adjoint methods.[6–8] It seems that the last class (the so-called ELLAM method) is very efficient but needs to be applied effectively in multiple dimensions and complex geometries and flows.[9]

Some words have to be said about the particle-tracking method based on a random walk process for the description of the diffusive part of the transport equation.[10–12] This approach is commonly used. It gives accurate results but incurs a high computational cost.[13]

In the context of a purely Eulerian approach, special schemes have been developed to solve hyperbolic equations with finite differences or finite elements. Upwind schemes which have been introduced in finite differences[14] give first-order-accurate stable schemes with no oscillations, but with too much numerical diffusion smearing the front. To overcome this problem, high-order-accurate and non-oscillatory finite difference upwind schemes have been developed.[15,16] These schemes are generally constructed through a discontinuous piecewise polynomial representation of the solution[17] and are stabilized with slope limiters. This step determines the linear distribution of the concentration in each element, without overshoots or undershoots with respect to neighbouring cell averages. The numerical flux at an interface is obtained by solving a local Riemann problem. The extension of these schemes to two space dimensions using quadrilateral control volumes is obtained by writing the one-dimensional scheme in directions parallel to the axes. With these elements it becomes difficult to calculate on domains with complex configurations.

Chakravarthy and Osher[18] extended such schemes to triangular elements using a finite volume approximation. Putti *et al.*[19] applied this method to the resolution of the general transport equation in a saturated porous medium. This scheme is second-order-accurate for equilateral triangles.

High-order schemes with multidimensional slope limiters have been developed using discontinuous finite elements by Chavent and Jaffre.[20] We report here on the adaptation of the latter to triangular elements for the discretization of the advective term. The dispersive term is approximated using a mixed hybrid finite element formulation.

In this paper we briefly present the discontinuous finite element method in one dimension and further extend this method to triangular elements in conjunction with the mixed hybrid approximation for the discretization of the diffusive term. The second part of the paper discusses some numerical results. We compare our technique with a classical mixed finite element method and with the high-order finite volume method developed by Putti *et al.*[19] using a two-dimensional analytical solution. Cases are presented for various cell Peclet numbers and CFL numbers and for regular and irregular meshes to test the robustness of this method.

THE DISCONTINUOUS FINITE ELEMENT SCHEME IN ONE DIMENSION

We consider here the flow of a fluid that carries an inert and neutral solute through a porous medium. Within the usual macroscopic approach the solute concentration (defined as mass of solute per

volume of fluid) satisfies the classical advection–diffusion equation. This advection–diffusion equation can be written as[21]

$$\frac{\partial c}{\partial t} = -\nabla \cdot (\vec{v}c) + \nabla \cdot (\mathbf{D} \cdot \nabla c) + G, \tag{1}$$

where c is the concentration of the contaminant ($\mathrm{M\ L^{-3}}$), $\vec{v}$ is the average pore water velocity vector ($\mathrm{L\ T^{-1}}$), $\mathbf{D}$ is the diffusion tensor ($\mathrm{L^2\ T^{-1}}$) and G is the source or sink terms ($\mathrm{M\ L^{-3}\ T^{-1}}$).

A discontinuous finite element method is used for the discretization of the advective terms. Without the diffusive terms, equation (1) becomes a hyperbolic equation:

$$\frac{\partial c}{\partial t} = -\nabla \cdot (\vec{v}c). \tag{2}$$

The one-dimensional space interval $[a, b]$ is discretized with a set of elements $K = [x_i, x_{i+1}]$ and nodes $x_1 = a < \ldots < x_{i+1} < \ldots < x_{1+1} = b$. We denote by Δx_K the size of element K.

The concentration c is approximated in a space of discontinuous linear functions, $M^1 = \{f|_K \in (m_{K1}, m_{K2})\}$. In other words, the restriction of f over K is a linear combination of m_{K1} and m_{K2}. The functions of M^1 are discontinuous at the nodes of discretization, so we denote by f_i^{in} and f_i^{out} the inside and outside limits respectively of a function in M^1 at node x_i with respect to element K.

The linear variation in c over K is defined as

$$c_K(x) = m_{K1}(x)c_i^{\text{in}} + m_{K2}(x)c_{i+1}^{\text{in}}, \tag{3}$$

where c_i^{in} is the inside limit value of c at node i with respect to K and c_{i+1}^{in} is the inside limit value of c at node $i+1$ with respect to K.

A variational form of the hyperbolic equation is obtained over element K:

$$\int_K \frac{\partial c}{\partial t} m \, \mathrm{d}x = -\int_K \nabla \cdot (\vec{v}c) m \, \mathrm{d}x, \tag{4}$$

where m is a test function ($\in M^1$ over K).

By using the Green formula, the following approximation equation is obtained:

$$\int_K \frac{\partial c_K}{\partial t} m \, \mathrm{d}x = \int_K \vec{v}_K c_K \cdot \nabla m \, \mathrm{d}x - Q_{K,i+1} c_{i+1}^{\text{in or out}} m(x_{i+1}) - Q_{K,i} c_i^{\text{in or out}} m(x_i), \tag{5}$$

where $Q_{K,i}$ is the flux at node i for element K. The out-flux is defined as positive and the in-flux as negative (this flux must be continuous at the interface of two adjacent elements).

To preserve mass balance, the advective fluxes have to be uniquely defined at the interface of two elements. A choice must be carried out at the interface between the discontinuous values c^{in} and c^{out}. The advective flux is obtained by solving a standard Riemann problem in the linear case. In other words, the numerical advective flux is calculated with the upstream value of c. The choice between the discontinuous values c^{in} and c^{out} depends on the sign of Q ($c_i = c_i^{\text{in}}$ if $Q_{K,i} > 0$ and $c_i = c_i^{\text{out}}$ if $Q_{K,i} < 0$) (see Figure 1).

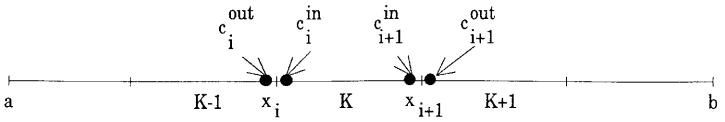

Figure 1. Discontinuous limit values of c at nodes x_i and x_{i+1}

We will use an explicit time discretization scheme. Considering $0 = t_0 \leqslant t_1 \leqslant \ldots \leqslant t_n \ldots$ and with $\Delta t_n = t_{n+1} - t_n$ a time discretization, equation (5) becomes

$$\int_K \frac{c_K^{n+1} - c_K^n}{\Delta t_n} m \, \mathrm{d}x = \int_K \vec{v}_K c_K^n \cdot \nabla m \, \mathrm{d}x - Q_{K,i+1} c_{i+1}^{\text{in or out},n} m(x_{i+1} - Q_{K,i} c_i^{\text{in or out},n} m(x_i). \tag{6}$$

By using successively m_{K1} and m_{K2} as test functions and solving the Riemann problem at the interfaces, a system of two unknowns per element, $c_{i+1}^{\text{in},n+1}$ and $c_i^{\text{in},n+1}$ (compounds of c_K^{n+1} in the bases m_{K1} and m_{K2}), is obtained. This scheme does not have good stability properties and the calculated solution oscillates.

To increase the time discretization accuracy, an intermediate time step at time $t_{n+1/2}$ is introduced. The advective fluxes are calculated using the concentration values defined inside element K.

Step 1. Calculation of $c^{n+1/2}$ with local values

$$\int_K \frac{c_K^{n+1/2} - c_K^n}{\frac{1}{2}\Delta t_n} m \, \mathrm{d}x = \int_K \vec{v}_K c_K n \cdot \nabla m \, \mathrm{d}x - Q_{K,i+1} c_{i+1}^{\text{in,n}} m(x_{i+1}) - Q_{K,i} c_i^{\text{in},n} m(x_i). \tag{7}$$

Step 2. Calculation of c_{n+1^*} by solving a Riemann problem

$$\int_K \frac{c_K^{n+1^*} - c_K^n}{\Delta t_n} m \, \mathrm{d}x = \int_K \vec{v}_K c_K^{n+1/2} \cdot \nabla m \, \mathrm{d}x - Q_{K,i+1} c_{i+1}^{\text{in or out},n+1/2} m(x_{i+1}) - Q_{K,i} c_i^{\text{in or out},n+1/2} m(x_i). \tag{8}$$

To stabilize this scheme, a slope-limiting step is introduced. The slope-limiting operator L associates with each function c^{n+1^*} $(\in M^1)$ a function $L(c^{n+1}$ $(\in M_1)$ which satisfies the following conditions.

(a) Preservation of mass balance by

$$\overline{c_K^{n+1}} = \int_K \frac{c_K^{n+1}}{\Delta x_K} \, \mathrm{d}x = \frac{c_i^{\text{in},n+1} + c_{i+1}^{\text{in},n+1}}{2} = \overline{c_K^{n+1^*}} = \frac{c_i^{\text{in},n+1^*}}{2}. \tag{9}$$

(b) Limitation of the slope by setting an upper and a lower limit value to $c_i^{\text{in},n+1}$ and $c_{i+1}^{\text{in},n+1}$:

$$(1-\theta)\overline{c_K^{n+1^*}} + \theta \min(\overline{c_{K-1}^{n+1^*}}, \overline{c_K^{n+1^*}}) \leqslant c_i^{\text{in},n+1} \leqslant (1-\theta)\overline{c_K^{n+1^*}} + \theta \max(\overline{c_{K-1}^{n+1^*}}, \overline{c_K^{n+1^*}}), \tag{10}$$

$$(1-\theta)\overline{c_K^{n+1^*}} + \theta \min(\overline{c_{K+1}^{n+1^*}}, \overline{c_K^{n+1^*}}) \leqslant c_{i+1}^{\text{in},n+1} \leqslant (1-\theta)\overline{c_K^{n+1^*}} + \theta \max(\overline{c_{K+1}^{n+1^*}}, \overline{c_K^{n+1^*}}), \tag{11}$$

where θ is a weighting parameter ($0 \leqslant \theta \leqslant 1$). (With $\theta = 1$ the previous relations specify that $c_i^{\text{in},n+1}$ and $c_{i+1}^{\text{in},n+1}$ have not to be greater or smaller than the mean concentration in the element $K-1, K, K+1$.)

Relations (10) and (11) imply that if $\overline{c_k^{n+1^*}}$, is a local minimum or maximum of c, then $c_i^{\text{in},n+1}$ and $c_{i+1}^{\text{in},n+1}$ are defined by

$$c_{i+1}^{\text{in},n+1} = c_i^{\text{in},n+1} = \overline{c_K^{n+1^*}} \quad \text{if } \overline{c_K^{n+1^*}} \geqslant \max(\overline{c_{K-1}^{n+1^*}} \overline{c_{K+1}^{N+1^*}}) \quad \text{or} \quad \overline{c_K^{n+1^*}} \leqslant \min \overline{c_{K+1}^{n+1^*}}). \tag{12}$$

If we are not in case (12) (i.e. it is not a local minimum or maximum for c), note that c_K^{n+1} is not uniquely defined by (9)–(11). To define it uniquely, we impose that c_K^{n+1} be as close as possible to

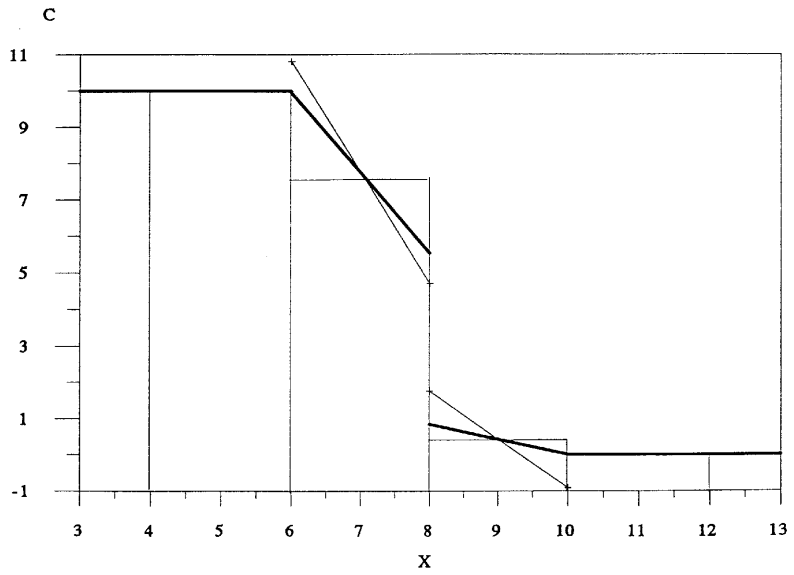

Figure 2. Slope-limiting effects: linear discontinous variation in concentration before (—) and after (▬) slope limiting

$c_K^{n+1^*}$. A minimization problem of dimension two has to be solved for the element K to determine c_K^{n+1}.

An objective function J_K is defined by

$$J_K(c_i^{\text{in},n+1}, c_{i+1}^{\text{in},n+1}) = \left\| c_i^{\text{in},n+1} - c_i^{\text{in},n+1^*} \right\|^2 + \left\| c_{i+1}^{\text{in},n+1} - c_{i+1}^{\text{in},n+1^*} \right\|^2. \tag{13}$$

Then $c_i^{\text{in},n+1}$ and $c_{i+1}^{\text{in},n+1}$ are estimated by minimizing the objective function J_K and satisfying the constraints (9)–(11). The slope-limiting effects can be visualized graphically as in Figure 2.

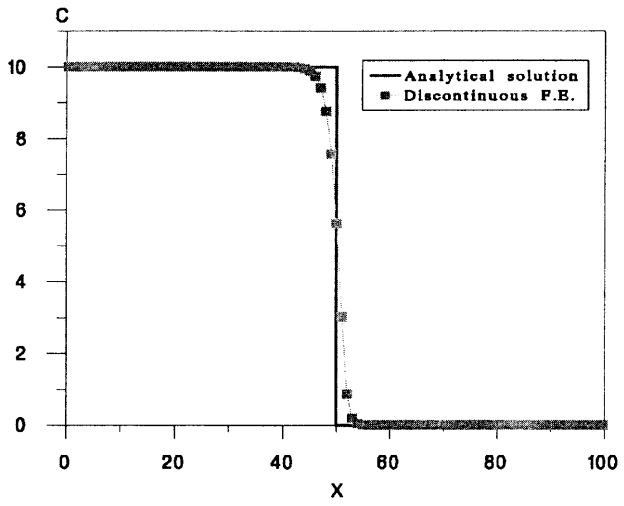

Figure 3. One-dimensional pure advection example

The discontinuous finite element method associated with this slope limiter is total-variation-diminishing (TVD) if the following criterion is respected:[22]

$$CFL \leqslant \max\left(\frac{1}{1+2\theta}, \frac{1}{2}\right) \quad \text{for every element } K,$$

CFL being the Courant–Friedrichs–Levy number equal to $v_K \Delta t/\Delta x_K$. The TVD property insures that the scheme does not produce non-physical oscillations. Moreover, the slope limiter introduces the smallest amount of numerical diffusion for θ unit to unity.[23] Figure 3 shows a numerical pure advection example. The discontinuous finite element method gives accurate results. In one dimension this method is very similar to the high-order finite difference method invented by Van Leer.[15] The discontinuous finite element method is more expensive compared with the high-order finite difference scheme in one dimension, but it can be easily extended in a true multidimensional scheme.

RESOLUTION OF THE ADVECTION–DIFFUSION EQUATION IN 2D WITH TRIANGULAR ELEMENTS

Approximation of the convective term

As previously, the convective term is approximated by a discontinuous finite element method. The two-dimensional domain is discretized with triangular elements K.

The concentration c is approximated in a space of discontinuous bilinear functions, $M_1 = \{f|_K \in (m_{K1}, m_{K2}, m_{K3})\}$, which means that the restriction of f over K is a linear combination of m_{K1}, m_{K2} and m_{K3}.

The functions of M^1 are discontinuous at nodes of discretization. By considering the triangular element K formed by nodes A, B and C, the variation in c over K can be written as

$$c_K(x, y) = m_{K1} c_{\mathrm{A}}^K + m_{K2} c_{\mathrm{B}}^K + m_{K3} c_{\mathrm{C}}^K, \tag{14}$$

where c_{A}^K is the value of c at node A in element K, c_{B}^K is the value of c at node B in element K and c_{C}^K is the value of c at node C in element K.

We denote by $c_{\mathrm{AB}}^{\mathrm{in}}$ the linear variation in c over edge AB in element K and $c_{\mathrm{AB}}^{\mathrm{out}}$ the linear variation in c over edge AB in the element adjacent to K. In order to simplify the notation, $\vec{v}$ and c (without index K) will denote the approximations of velocity and concentration over element K respectively. Second-order time discretization is used to solve the hyperbolic equation (2).

Step 1. calculation of $\mathrm{c}^{\mathrm{n}+1/2}$ *with local values*

$$\int_K \frac{c^{n+1/2} - c^n}{\frac{1}{2}\Delta t_n} m \, \mathrm{d}x = \int_K \vec{v} c^n \cdot \nabla m \, \mathrm{d}x - Q_{K,\mathrm{AB}} \int_{\mathrm{AB}} \frac{c_{\mathrm{AB}}^{\mathrm{in},n} m}{\overline{\mathrm{AB}}} \, \mathrm{d}s$$
$$- Q_{K,\mathrm{BC}} \int_{\mathrm{BC}} \frac{c_{\mathrm{BC}}^{\mathrm{in},n} m}{\overline{\mathrm{BC}}\, \mathrm{d}s} - Q_{K,\mathrm{CA}} \int_{\mathrm{CA}} \frac{c_{\mathrm{CA}}^{\mathrm{in},n} m}{\overline{\mathrm{CA}}} \, \mathrm{d}s, \tag{15}$$

where m is a test function of M^1 over K, $\overline{AB}$ (respectively $\overline{BC}$ and $\overline{CA}$) is the length of edge AB (respectively BC and CA) and $Q_{K,\mathrm{AB}}$ is the flux through edge AB with respect to $\vec{n}_{K,\mathrm{AB}}$, the latter being the unit exterior normal vector of this edge for element K ($\mathrm{sign}(Q_{K,\mathrm{AB}}) = \mathrm{sign}(\vec{n}_{K,\mathrm{AB}} \cdot \vec{v})$). The flux is continuous at the interface of two adjacent elements K and K' ($Q_{K,\mathrm{AB}} + Q_{K'\mathrm{AB}} = 0$).

By using successively the three basis functions of M^1 over K as test functions, we obtain a system of three unknowns per element K. The values at each node in K are calculated by solving this local system.

Step 2. Calculation of c^{n+1^*} by solving the Riemann problem

$$\int_K \frac{c^{n+1^*}-c^n}{\Delta t_n} m \, \mathrm{d}x = \int_K \vec{v}c^{n+1/2} \cdot \nabla m \, \mathrm{d}x - Q_{K,\mathrm{AB}} \int_{\mathrm{AB}} \frac{c_{\mathrm{AB}}^{\text{in or out},n+1/2} m}{\overline{\mathrm{AB}}} \, \mathrm{d}s - Q_{K,\mathrm{BC}} \int_{\mathrm{BC}} \frac{c_{\mathrm{BC}}^{\text{in or out},n+1/2} m}{\overline{BC}} \, \mathrm{d}s - Q_{K,\mathrm{CA}} \int_{\mathrm{CA}} \frac{c_{\mathrm{CA}}^{\text{in or out},n+1/2} m}{\overline{\mathrm{CA}}} \, \mathrm{d}s. \quad (16)$$

In this step the numerical advective flux is calculated with the upstream 'value' of c over the interface of two elements. The choice between $c_{\mathrm{AB}}^{\mathrm{in}}$ and $c_{\mathrm{AB}}^{\mathrm{out}}$ depends on the sign of $Q_{K,\mathrm{AB}}$.

(a) If $Q_{K,\mathrm{AB}} \geqslant 0$, then $c_{\mathrm{AB}} = c_{\mathrm{AB}}^{\mathrm{in}}$.
(b) If $Q_{K,\mathrm{AB}} < 0$, then $c_{\mathrm{AB}} = c_{\mathrm{AB}}^{\mathrm{out}}$.

The scheme is stabilized with multidimensional slope limiters (extension of the one-dimensional slope limiter). For element K we introduce the following notation.

(a) $\overline{c_K}$ is the average of c over K: $\overline{c_K} = (c_{\mathrm{A}}^K + c_{\mathrm{B}}^K + c_{\mathrm{C}}^K)/3$.
(b) min(A) is the minimum of the $\overline{c_K^{n+1^*}}$ of all elements having A for a node.
(c) max(A) is the maximum of the $\overline{c_K^{n+1^*}}$ of all elements having A for a node.
(d) min(K) is the minimum of the $\overline{c_K^{n+1^*}}$ of all elements having a common node with element K.
(e) max(K) is the maximum of the $\overline{c_K^{n+1^*}}$ of all elements having a common node with element K.

The multidimensional slope-limiting operator $\boldsymbol{L}$ associates with each function c^{n+1^*} ($\in M^1$) a function $\boldsymbol{L}(c^{n+1^*}) = c^{n+1}$ ($\in M^1$) satisfying the following conditions. In order to preserve mass balance,

$$\overline{c_K^{n+1}} = \overline{c_K^{n+1^*}}. \quad (17)$$

In order to limit the variation,

$$\min(A) \leqslant c_{\mathrm{A}}^{K,n+1} \leqslant \max(\mathrm{A}), \quad (18)$$

$$\min(\mathrm{B}) \leqslant c_{\mathrm{B}}^{K,n+1} \leqslant \max(\mathrm{B}), \quad (19)$$

$$\min(\mathrm{C}) \leqslant c_{\mathrm{C}}^{k,n+1} \leqslant \max(\mathrm{C}). \quad (20)$$

When $c_K^{n+1^*}$ corresponds to a local maximum of c in K, then relations (17)–(20) imply that

$$c_{\mathrm{A}}^{K,n+1} = c_{\mathrm{B}}^{K,n+1} = c_{\mathrm{C}}^{K,n+1} = \overline{c_{\mathrm{K}}^{n+1^*}} \quad \text{if } \overline{c_K^{n+1^*}} \geqslant \max(K) \text{ or } \overline{c_K^{n+1^*}} \leqslant K \min(K). \quad (21)$$

If we are not in case (21), c_K^{n+1} is not uniquely defined. We impose that c_K^{n+1} be as close as possible to $c_K^{n+1^*}$. A minimization problem of dimension three has to be solved for the element to determine c_K^{n+1}.

An objective function J is defined by

$$J(c_{\mathrm{A}}^{K,n+1}, c_{\mathrm{B}}^{K,n+1}, c_{\mathrm{C}}^{K,n+1}) = \left\| c_{\mathrm{A}}^{K,n+1} - c_{\mathrm{A}}^{K,n+1*} \right\|^2 + \left\| c_{\mathrm{B}}^{K,n+1} - c_{\mathrm{B}}^{K,n+1*} \right\|^2 + \left\| c_{\mathrm{C}}^{K,n+1} - c_{\mathrm{C}}^{K,n+1*} \right\|^2. \quad (22)$$

Then $c_{\mathrm{A}}^{K,n+1}$, $c_{\mathrm{B}}^{K,n+1}$ and $c_{\mathrm{C}}^{K,n+1}$ are estimated by minimizing the objective function J and satisfying the constraints (17)–(20). The method used to solve this minimization problem is the saddle point method.[24]

Approximation of the diffusive term

The diffusive term is discretized with a mixed approximation.[20] We introduce the diffusive flux $\vec{q}_{\mathrm{d}} = -\mathbf{D} \cdot \nabla c$. On each element K, c and $\vec{q}_{\mathrm{d}}$ are approached by an approximation of

(a) the average of c on K: $\overline{c_K}$
(b) the average of c along each edge E_i of K, denoted $TC_{K,i}$ for $i = 1, 2, 3$
(c) $\vec{q}\mathrm{d} = -\mathbf{D} \cdot \nabla c$, noted $\vec{q}_{\mathrm{d},K}$.

$\vec{q}_{\mathrm{d},K}$ has the following properties over K.[25,26]

(a) $\nabla \cdot \vec{q}_{\mathrm{d},K}$ is constant over K.
(b) $\forall i = 1, 2, 3, \vec{q}_{\mathrm{d}} \cdot \vec{n}_{Ki}$ is constnat over face E_i, $\vec{n}_{Ki}$ being the unit exterior normal vector of edge E_i.
(c) $\vec{q}_{\mathrm{d},K}$ is perfectly determined by the knowledge of its flux $Q_{\mathrm{d},K,i}$ through edge $E_i (i = 1, 2, 3)$.

The diffusive flux can be calculated using basis vectorial functions $(\vec{w}_i)_{i=1,2,3}$ defined by

$$\int_{E_j} \vec{w}_i \cdot \vec{n}_{Kj} \, \mathrm{d}s = \delta_{ij} \quad \text{for } j = 1, 2, 3,$$

where δ_{ij} is the Kronecker symbol.

The vector $\vec{w}_i$ corresponds to a vector with a flux of unity through edge E_i and zero flux through the others. The expressions of the basis functions are given e.g. by Chavent and Roberts.[27] Any vector $\vec{q}_{\mathrm{d},K}$ can be written as a linear combination of $(\vec{w}_i)_{i=1,2,3}$:

$$\vec{q}_{\mathrm{d},K} = \sum_{j=1}^{3} Q_{\mathrm{d},K,j} \vec{w}_j.$$

The expression of $\vec{q}_{\mathrm{d},K}$ is then written in variational form over each element K:

$$\int_K (\mathbf{D}^{-1} \cdot \vec{q}_{\mathrm{d},K}) \cdot \vec{s} \, \mathrm{d}x = -\int_K \nabla c \cdot \vec{s} \, \mathrm{d}x, \tag{23}$$

where $\bar{s}$ is a sufficient regular test function.

By carrying out the same calculations as Chavent and Roberts,[27] we obtain approximation equation

$$\sum_{j=1}^{3} B_{ij} Q_{\mathrm{d},K,j} = \overline{c_K} - TC_{K,i} \quad \forall i = 1, 2, 3, \tag{24}$$

where

$$B_{ij} = \int_K [(\mathbf{D}_K^{-1} \cdot \overline{w}_j) \cdot \overline{w}_i] \, \mathrm{d}x.$$

If we define the symmetric 3×3 matrix B_K associated with element K as $B_K = [B_{ij}]$ (which is invertible), the previous equation becomes in matrix form

$$Q_{\mathrm{d},K} = B_K^{-1}(\overline{c_K} DIV_K^{\mathrm{T}} - TC_K), \tag{25}$$

where

$$DIV_K^{\mathrm{T}} = [\text{elementary divergence matrix}]^{\mathrm{T}} = \begin{bmatrix} 1 \\ 1 \\ 1 \end{bmatrix},$$

$$Q_{\mathrm{d},K} = [Q_{\mathrm{d},K,i}], \qquad TC_K = [TC_{K,i}], \qquad B_K = [B_{ij}].$$

By using an index notation referring to the edges, the components of $Q_{\mathrm{d},K}$ are

$$Q_{\mathrm{d},K,E} = \overline{c_K} \alpha_{K,E} - \sum_{I \subset K} B^{-1}_{K,E,E'} TC_{K,E'}, \quad \text{with } \alpha_{K,E} = \sum_{E \subset K} B^{-1}_{K,E,E'} \tag{26}$$

where $\sum_{E \subset K}$ denotes a sum over the edges E of K.

By using the continuity of the diffusive fluxes (i.e. $Q_{\mathrm{d},K,E} + Q_{\mathrm{d},K'E} = 0$ for every edge E, K and K' being adjacent) and equation (26), the following relation can be obtained:

$$\alpha_{K,E}\overline{c_K} + \alpha_{K'E}\overline{c_{K'}} - \sum_{E'\subset K} B^{-1}_{K,E,E'}\, TC_{E'} - \sum_{E'\subset K'} B^{-1}_{K',E,E'}\, TC_{E'} = 0. \tag{27}$$

This equation is written in matrix form as

$$M\mathbf{C} - N\mathbf{TC} - \mathbf{I} = 0, \tag{28}$$

where **TC** is the vector formed by the TC_E $\forall E \notin$ Dirichlet-type boundary, **C** is the vector formed by the $\overline{c_K}$,

$$M = [M_{E,K}]_{ne,nk}, \quad \text{with } M_{E,K} = \begin{cases} \alpha_{K,E} & \text{if } E \subset K, \\ 0 & \text{if } E \not\subset K, \end{cases}$$

$$N = [N_{E,E'}]_{ne,ne}, \quad \text{with } N_{E,E'} = \sum_{K\supset E \text{ and } E'} B^{-1}_{K,E,E'},$$

where $\sum_{K\supset E \text{ and } E'}$ denotes a sum over the elements K containing edges E and E', and

$$\mathbf{I} = [I_E]_{ne}, \quad \text{with } I_E = \sum_{E'\subset(K\supset E)} B_{K,E,E'}\, TC_{E'} \quad \forall E' \in \text{Dirichlet-type boundary}.$$

The numbers *ne* and *nk* are the number of edges and the number of elements respectively. With this matrix relation we can determine **TC** from **C** by solving the linear equation system whose associated matrix N is symmetric positive definite:

$$N\mathbf{TC} = M\mathbf{C} - \mathbf{I}. \tag{29}$$

This system is solved efficiently by a standard method such as a preconditioned conjugate gradient method.

The diffusive term $\nabla\cdot\vec{q}_{\mathrm{c}} = -\nabla\cdot(\mathbf{D}\nabla c)$ is then discretized at time t_n by

$$\int_K \nabla\cdot\vec{q}^{\,n}_{\mathrm{d},K} = \int_K \nabla\cdot\left(\sum_{E\subset K} Q^n_{\mathrm{d},K,E}\vec{w}_E\right) = \sum_{E\subset K} Q^n_{\mathrm{d},K,E}\int_E \vec{w}_E\cdot\vec{n}_E = \sum_{E\subset K} Q^n_{\mathrm{d},K,E}. \tag{30}$$

$\nabla\cdot\vec{q}^{\,n}_{\mathrm{d},K}$ being constant over K, equation (30) can be written as

$$\nabla\cdot\vec{q}^{\,n}_{\mathrm{d},K} = \frac{1}{|K|}\sum_{E\subset K} Q^n_{\mathrm{d},K,E} \tag{31}$$

where $|K|$ is the area of element K.

Plugging equation (26) into (31) gives immediately

$$\nabla\cdot\vec{q}^{\,n}_{\mathrm{d},K} = \frac{1}{|K|}\left(\alpha_K\overline{c^n_K} - \sum_{E'\subset K}(\alpha_{K,E'}TC^n_{K,E'})\right), \tag{32}$$

with

$$\alpha_{K,E} = \sum_{E'\subset K} B^{-1}_{K,E,E'}\,, \qquad \alpha_K = \sum_{E\subset K}\alpha_{K,E}.$$

Complete solution of the convection–diffusion equation

We now combine the discontinuous finite elements and mixed finite elements for the resolution of the advection–diffusion equation (1). The initial values of the concentration have to be determined for the edges and for the nodes in each element.

Step 1. Calculation of $c^{n+1/2}$ *with local values. The diffusive terms (32) are introduced into equation (15):*

$$\int_K \frac{c^{n+1/2}-c^n}{\frac{1}{2}\Delta t_n} m = \int_K \vec{v}c^n \cdot \nabla m - Q_{K,\mathrm{AB}} \int_{\mathrm{AB}} \frac{c_{\mathrm{AB}}^{\mathrm{in},n} m}{\overline{AB}}\, \mathrm{d}s - Q_{K,\mathrm{BC}} \int_{\mathrm{BC}} \frac{c_{\mathrm{BC}}^{\mathrm{in},n} m}{\overline{\mathrm{BC}}}\, \mathrm{d}s - Q_{K,\mathrm{CA}} \int_{\mathrm{CA}} \frac{c_{\mathrm{CA}}^{\mathrm{in},n} m}{\overline{\mathrm{CA}}}\, \mathrm{d}s - \frac{1}{|K|}\left(\alpha_K \overline{c_K^n} - \sum_{E' \subset K} (\alpha_{K,E'} TC_{K,E'}^n)\right) \int_K m + G \int_K m, \tag{33}$$

where m is successively one of the three basis functions of M^1 over K.

The value at time $t_{n+1/2}$ at each node in K is easily calculated by solving a local system. We determine then the value of $c_K^{n+1,2}$ and the average of c over K. The concentrations per edge, $TC^{n+1/2}$, are calculated from $c_K^{n+1/2}$ by solving system (29).

Step 2. Calculation of c^{n+1^*} *by solving the Riemann problem*

$$\int_K \frac{c^{n+1^*}-c^n}{\Delta t_n} m = \int_K \vec{v}c^{n+1/2} \cdot \nabla m - Q_{K,\mathrm{AB}} \int_{\mathrm{AB}} \frac{c_{\mathrm{AB}}^{\text{in or out},n+1/2} m}{\overline{\mathrm{AB}}}\, \mathrm{d}s - Q_{K,\mathrm{BC}} \int_{\mathrm{BC}} \frac{c_{\mathrm{BC}}^{\text{in or out},n+1/2} m}{\overline{\mathrm{BC}}}\, \mathrm{d}s - Q_{K,\mathrm{CA}} \int_{\mathrm{CA}} \frac{c_{\mathrm{CA}^{\text{in or out},}n+1/2} m}{\overline{\mathrm{CA}}}\, \mathrm{d}s - \frac{1}{|K|}\left(\alpha_K \overline{c_K^{n+1/2}} - \sum_{E' \subset K} (\alpha_{K,E'} TC_{K,E'}^{n+1/2})\right) \int_K m + G \int_K m, \tag{34}$$

where m is successively one of the three basis functions of M^1.

The values at each node in K are calculated by solving a local system.

Step 3. Slope limitation. We calculate c_K^{n+1} satisfying (17)–(21) as close as possible to $c_K^{n+1^*}$. The concentrations per edge, TC^{n+1}, are then calculated from $\overline{c_K^{n+1}}$ by solving system (29).

With this method the mass balance is exact over each element K. The advective fluxes are uniquely defined by solving a Riemann problem at the interface of two elements. The dispersive flux is continuous from one element to the adjacent one. Dirichlet boundary conditions have to be imposed for the edges and for the nodes per element. This technique has been developed for any kind of triangular elements: regular (equilateral) or irregular. The accuracy and robustness of the method are now tested in two comparison studies. This method will be referred to as the discontinuous finite element method.

COMPARISON STUDIES

Test problem 1

In the first test problem the transport of a pulse in a rectangular two-dimensional region (Figure 4) is modelled for a pure advection problem. The flow is assumed to be uniform. The mesh being regular, this problem has the advantages that the transport occurs at various angles and the Courant number is not constant over the simulation domain. With the irregular mesh we test the robustness of the scheme presented here against the high-order finite volume method developed by Putti *et al.*[19] Their approach is based on a finite volume formulation and an implementation of a high-resolution

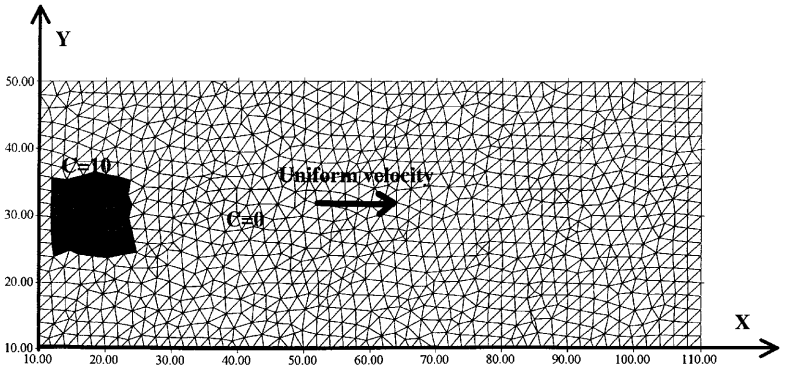

Figure 4. Advection of a pulse in an irregular mesh

upwind scheme for the discretization of the convective fluxes. By defining triangular cells, this scheme seems to be very attractive.

Figure 4 also illustrates the pulse with an initial height of 10 units at the beginning of the simulation. Figure 5 shows the transport of the pulse just before reaching the limit of the domain with

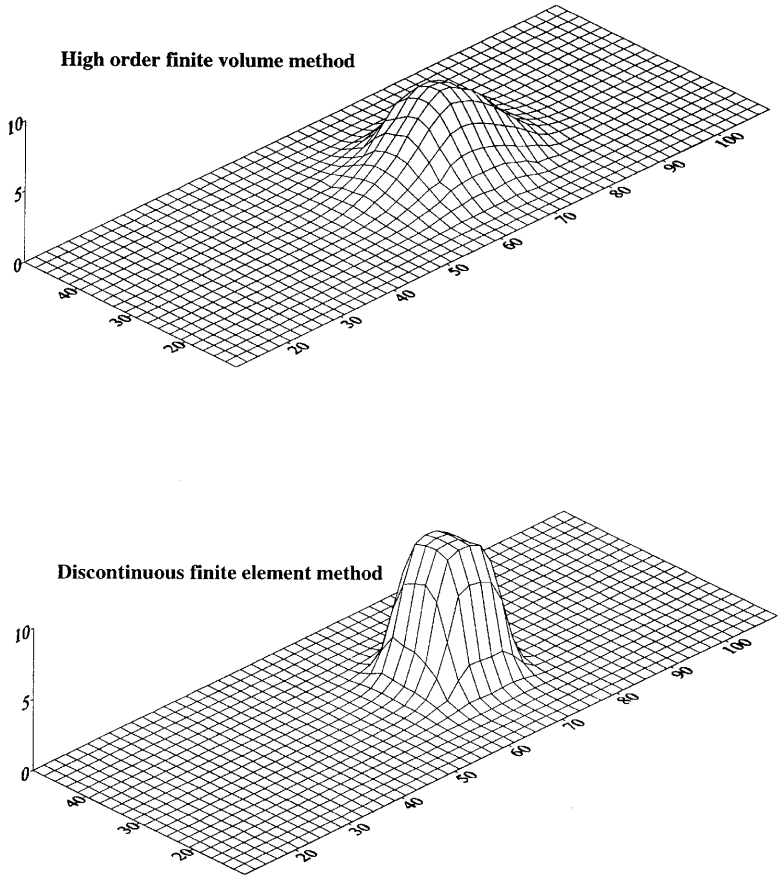

Figure 5. Pulse shape after displacement in domain for $Pe = \infty$

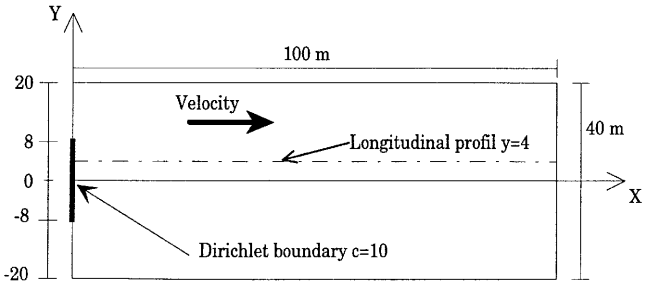

Figure 6. Two-dimensional convection–diffusion problem

the two methods. As mentioned by Putti *et al.*,[19] their scheme destroys the accuracy when non-equilateral triangles are considered. What is surprising is how the accuracy is lost on this example.

Test problem 2

For the second application we compare our scheme with the high-order finite volume method of Putti *et al.*[19] and with a classical finite element method. These numerical methods are verified against a two-dimensional analytical solution corresponding to the following conditions (Figure 6).

(a) The domain is homogeneous.
(b) The flow is one-dimensional and steady state; the pore velocity v is parallel to the x-axis.
(c) The initial condition is zero initial concentration.
(d) The boundary condition is a Dirichlet condition: $c(0, y, t > 0) = c_0$ if $|y| < a$ (in our case $a = 8$ m).

The analytical solution for this case is given by Leij Feike and Dane.[28] To compare the accuracy of the different methods, this problem is solved for various values of the grid Peclet number (designated *Pe*) as defined by Putti *et al.*[19] The solution of this problem is shown at time $t = 50$ s. The parameters used in the different cases are reported in Table I. Regular (Figure 7) and irregular (the same as the one used in the first case study, Figure 4) meshes are used to study mesh effects on the numerical results.

In the first case the transport is diffusion-dominated ($Pe \leqslant 2$). This case can be easily solved with the classical methods (conforming finite elements, mixed finite elements or finite differences). We did verify that the solution obtained with the discontinuous finite element method and the irregular grid agrees well with the analytical solution (Figure 8).

The second case is advection-dominated ($Pe = 10$). Longitudinal profiles at $y = 4$ m are used to see the effects of both longitudinal and transverse diffusion. The solutions obtained for the regular mesh with the high-order finite volume method and the discontinuous finite element method are very close to the analytical solution (Figure 9). The concentration front is well described. The results

Table I. Parameters used in various cases

Case	$v(x)$ (m s^{-1})	$v(y)$ (m s^{-1})	D_L (m^2 s^{-1})	D_T (m^2 s^{-1})	Δx (m)	Δy (m)	*Pe*
1	1·0	0·0	2	0·2	2·0	2·0	1
2	1·0	0·0	0·2	0·02	2·0	2·0	10
3	1·0	0·0	2×10^{-5}	2×10^{-6}	2·0	2·0	10000

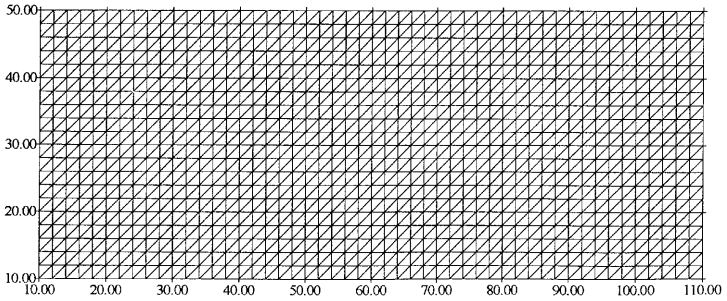

Figure 7. Regular mesh

obtained with the mixed approximation show oscillations (Figure 10). The data show a well-known result: the 'classical' methods are not adapted to approximate an advection-dominated transport equation. With the irregular mesh the discontinuous finite element method gives accurate results (Figure 11). On the other hand the high-order finite volume method now introduces longitudinal diffusion and transverse artificial diffusion (Figure 12).

The third case is a more advection-dominated case with $Pe = 10,000$. On the profile $y = 4$ with the two high-order methods (finite volume and discontinuous finite element approaches) no significant numerical diffusion appears for the regular mesh. With the irregular mesh the solution of the high-order finite volume method shows longitudinal diffusion (Figure 13). Good results were obtained with the discontinuous finite element method and the irregular mesh (Figure 13).

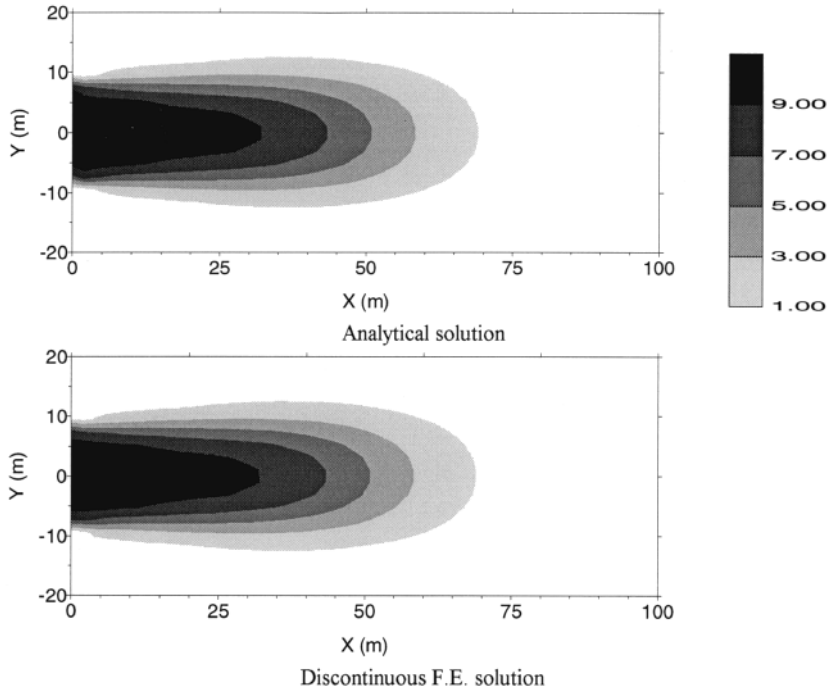

Figure 8. Analytical solution for diffusion-dominated case and computational results given by discontinuous finite element method with irregular mesh

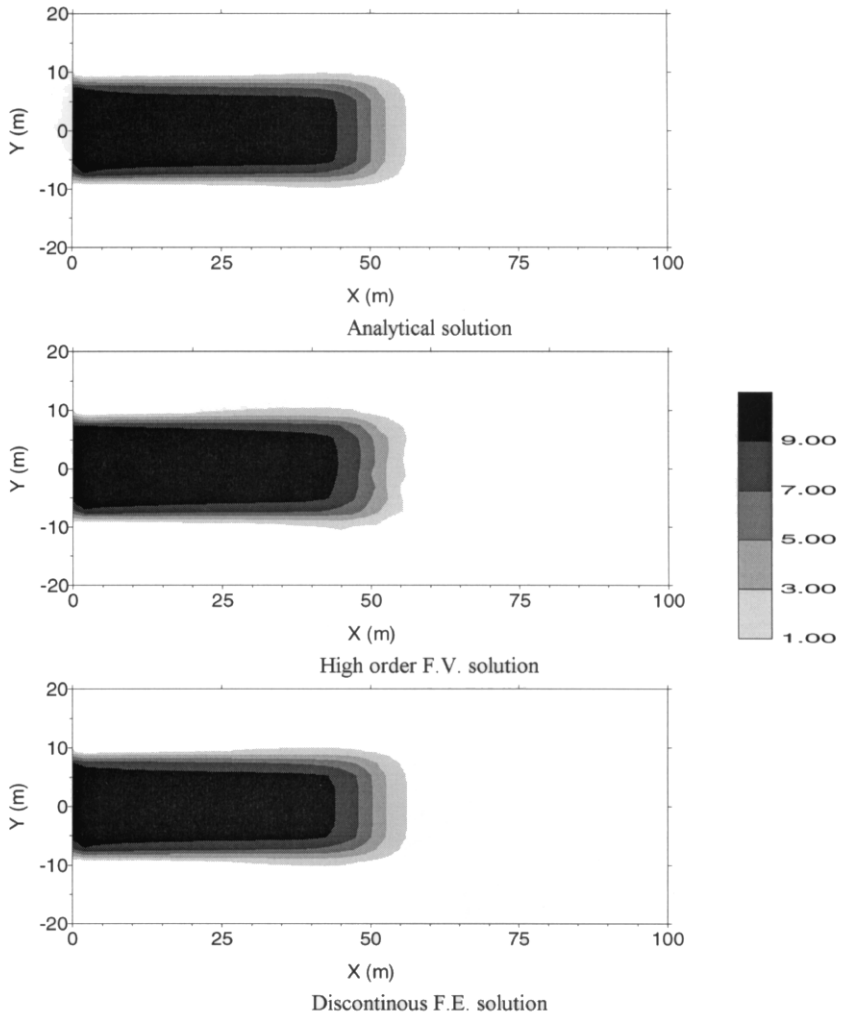

Figure 9. Comparison of results given by two high-order numerical methods (with regular mesh) and analytical solution for $Pe = 10$

To see the effects of the time step on the numerical results of the two high-order methods, the third case ($Pe = 10{,}000$) was studied with the regular mesh. Figures 14 and 15 show the numerical results obtained with both methods for various Courant–Friedrich's–Levy numbers.

For a linear convective flux and triangular elements, *CFL* can be defined as[19]

$$CFL_{\mathrm{p}} = \frac{1}{2}\frac{\oint_{\partial K} |\vec{v} \cdot \vec{n}| \mathrm{d}s}{|K|}\Delta t. \tag{35}$$

This is a possible calculation for *CFL* with triangular elements, but other definitions are available. For example, Kaddouri[29] proposes the formula $CFL_{\mathrm{k}} = (\| \vec{v} \| \times \Delta t)/h$, h being the ratio between the surface and perimeter of the triangle and $\| \vec{v} \|$ the norm of the velocity. Of course the stability criterion depends on the choice of the *CFL* definition.

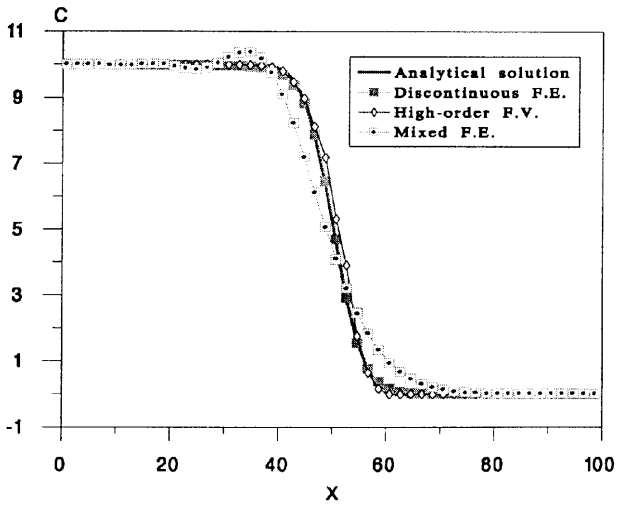

Figure 10. Comparison of results given by two high-order numerical methods (with regular mesh), mixed method and analytical solution using profile $y = 4$ (for $Pe = 10$

With a choice of $\theta = 1$ (which introduces the smallest amount of numerical diffusion in the slope limitation associated with the discontinuous finite elements), numerical experiments suggest that the scheme is stable for $CFL_p \leqslant 0{\cdot}9$. The algorithm proposed by Putti *et al.*[19] gives accurate results for $CFL_p = 1$. The concentration front is indeed well described with the high-order finite volume method

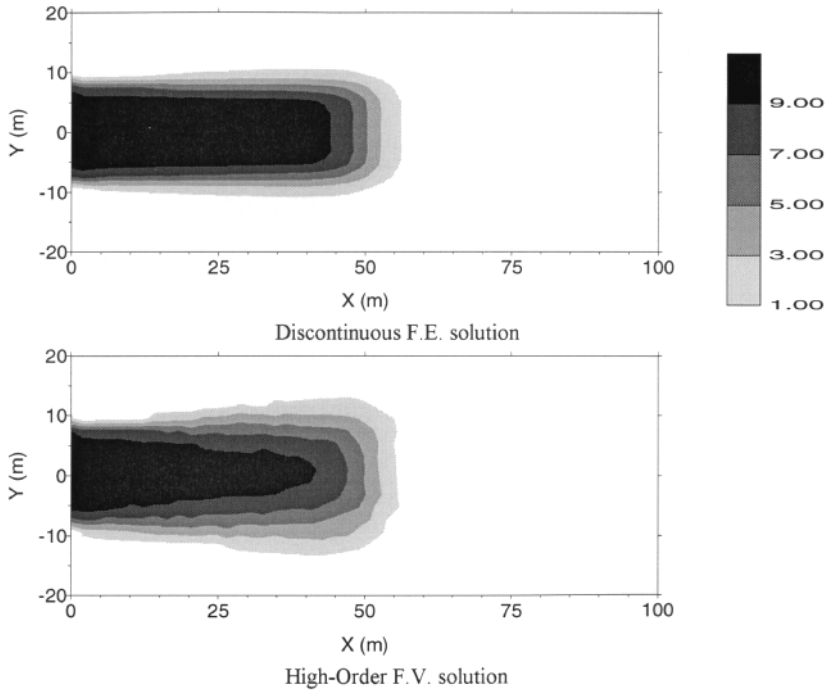

Figure 11. Comparison of results given by two high-order numerical methods with irregular mesh (for $Pe = 10$)

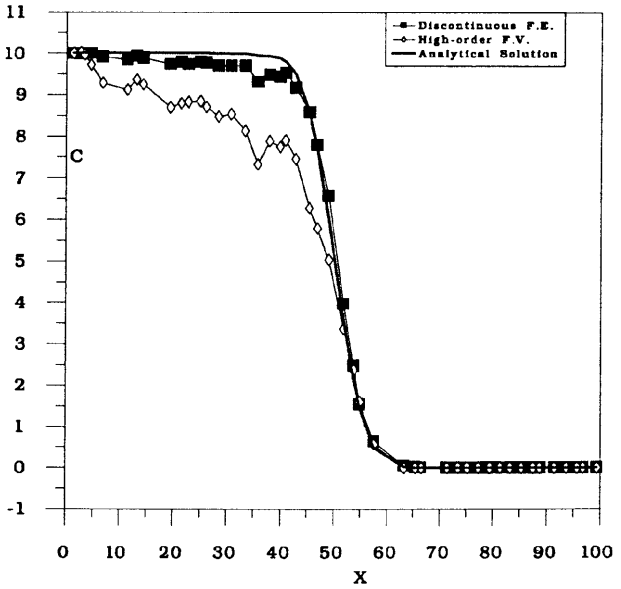

Figure 12. Comparison of results given by two high-order numerical methods (with irregular mesh) and analytical solution using profile $y = 4$ (for $Pe = 10$)

for $CFL_p = 1$ (Figure 14). Numerical diffusion appears with this scheme when CFL_p goes away from unity (Figure 14). With the discontinuous finite element method the concentration front is well described for the various CFL_p (Figure 15), but with the restriction of $CFL_p \leqslant 0{\cdot}9$. Only small diffusion appears when CFL_p is far from 0·9: this is certainly due to the fact that we use a

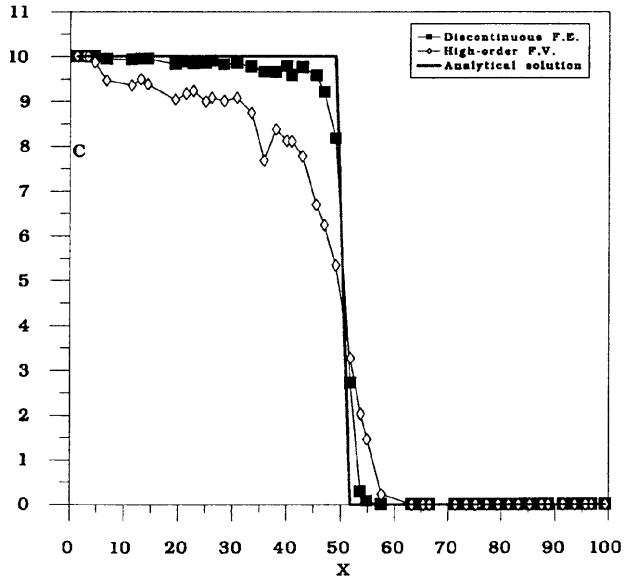

Figure 13. Comparison of results given by two high-order numerical methods (with irregular mesh) and analytical solution using profile $y = 4$ (for $Pe = 100,000$)

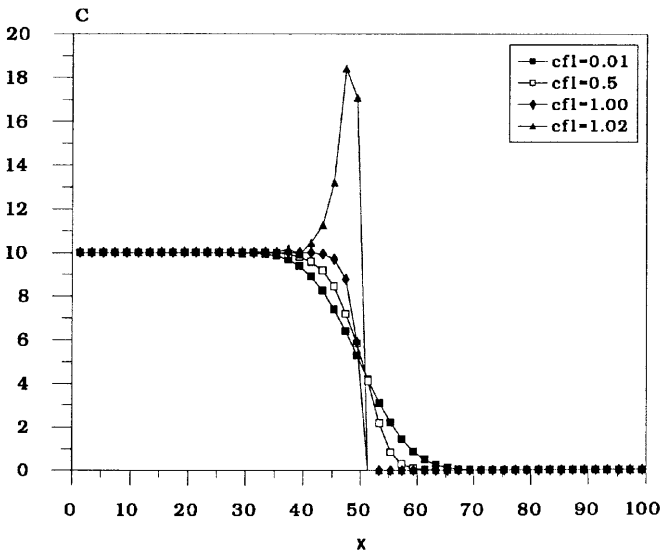

Figure 14. Effects of time step on numerical results given by high-order finite volume method

discontinuous formulation for the description of the concentration in each element. The presented scheme is unstable for $CFL_p = 1$ (Figure 15).

The discontinuous finite element method is well adapted to the modelization of real cases where the velocity is not constant in the domain. In our example this is not the case of the high-order finite volume method: the numerical results obtained with this method seem to be very sensitive to any variation in space of *CFL*.

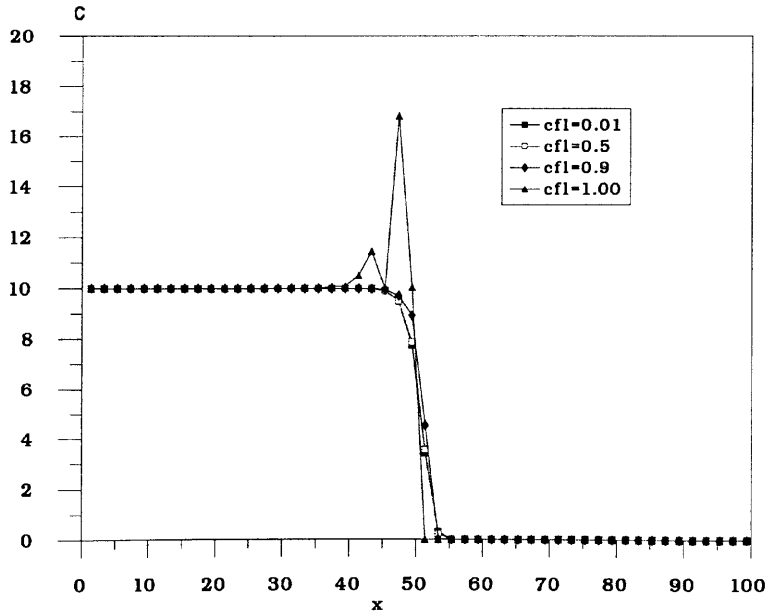

Figure 15. Effects of time step on numerical results given by discontinuous finite element method

CONCLUSIONS

A method based on discontinuous finite elements for the discretization of the advective term and mixed approximation for the diffusive term is presented for the numerical solution of the solute transport equation in a porous medium. With the discontinuous finite element method the advective fluxes are uniquely defined by solving a Rieman problem at the interface of two elements. This method stabilized with a slope limiter is especially adapted to the resolution of hyperbolic equations. The slope limiter introduces small amounts of numerical diffusion when sharp concentration fronts occur. With the mixed approximation the diffusive flux is continuous from one element to the adjacent one and the mass balance is exact over the element. The introduction of the mixed diffusive term in this method requires the resolution of a linear equation system whose associated matrix is symmetric positive definite. This operation increases the computational cost compared with classical high-order finite difference schemes. The combination of these two methods can be applied to 2D and 3D models using different types of elements with regular and irregular meshes. A two-dimensional scheme is developed using triangular elements.

With this smooth, numerical oscillations are completely avoided fro the full range of grid Peclet numbers. Numerical tests show good agreement with 1D and 2D analytical solutions. This approach is compared at the same time with two numerical methods, namely a mixed finite element method and a finite volume approach with high-resolution upwind terms. Regular and irregular meshes are used for the numerical tests to study mesh effects on the numerical results. The irregular mesh destroys the global second-order accuracy of the high-order finite volume scheme. The discontinuous finite element method performs well with triangles of any shape and for the full range of Peclet numbers. The discontinuous finite element method is not very sensitive to the variation in *CFL* (with the restriction of $CFL \leqslant 0.9$ if *CFL* is defined by equation (35)) compared with the high-order finite volume scheme, where *CFL* has to be as close as possible to unity.

In practical situations the presented algorithm is very useful as long as the mass transport is more and more solved in strongly heterogeneous media and the transport equation consequently becomes advection-dominated.

REFERENCES

1. P. S. Hukaykorn and G. F. Pinder, *Computational Methods in Subsurface Flow*, Academic, San Diego, CA, 1983.
2. A. O. Garder, D. W. Peacemann and A. L. Pozzi, 'Numerical calculations of multidimensional miscible displacement by the method of characteristics', *Soc. Pet. Eng.*, **4**, 26–36 (1964).
3. L. F. Konikow and J. D. Bredehoeft, 'Computer model of two-dimensional solute transport and dispersion in groundwater', *Techniques of Water-Resource Investigation of the United States Geological Survey, Book 7, Chapter C2*, United States Government Printing Office, Washington, DC 1978.
4. J. Douglas Jr. and T. F. Russell, 'Numerical methods for convection–diffusion problems based on combining the method of characteristics with finite element or finite difference procedures', *SIAM J. Numer. Anal.*, **19**, 871–885 (1982).
5. S. P. Neumann, 'A Eulerian–Lagrangian numerical scheme for the dispersion convection equation using conjugate space time grids', *J. Comput. Phys.*, **41**, 270–294 (1981).
6. T. F. Russell, 'Eulerian–Lagrangian localized adjoint methods for advection-dominated problems', *Proc. 13th Bienn. Conf. on Numerical Analysis*, Pitman, Dundee, 1989.
7. M. A. Celia, 'Eulerian–Lagrangian localized adjoint methods for contaminant transport simulations', *Proc. 10th Int. Conf. on Computational Methods in Water Resources*, Kluwer, Dordrecht, 1994.
8. M. A. Celia, T. F. Russell, I. Herrera and R. E. Ewing, 'An Eulerian–Lagrangian localized adjoint method for the advection diffusion equation', *Adv. Water Resources*, **13**, 187–206 (1990).
9. A. Oliveira and A. M. Baptista, 'A comparison of integration and interpolation Eulerian–Lagrangian methods', *Int. j. numer methods fluids*, **21**, 183–204 (1995).
10. Ph. Ackerer and W. Kinzelbach, 'Modélisation du transport de contaminant par la méthode de marche au hasard: influence des variations du champ d'écoulement au cours du temps sur la dispersion', *Proc. Symp. Int. sur l'Approache Stochastique des Ecoulments Souterrains*, Montvillargenne, 1985, pp. 446–458.

11. T. A. Prickett, T. G. Naymik and C. G. Lonquist, 'A random walk solute transport model for selected groundwater qulaityb evaluations', *Illinois State Water Survey, Bull. 65*, 1981.
12. G. J. M. Uffink, 'Analysis of dispersion by the random walk method', *Ph.D. Thesis*, Delft University, 1990.
13. W. Kinzelbach, *Numerische Methoden zur Modellierung des Transports von Schadstoffen im Grundwasser*, 2. Aufl, Oldenbourg, 1992.
14. R. Peyret and T. D. Taylor, *Computational Methods for Fluid Flow*, Springer, New York, 1983.
15. V. van Leer, 'Towards the ultimate conservative scheme: IV. A new approach to numerical convection', *J. Comput. Phys.*, **23**, 276–299 (1977).
16. P. L. Roe, 'Characteristic-based schemes for the Euler equation', *Ann. Rev. Fluid Mech.*, **18**, 337–365 (1986).
17. V. Van Leer, 'Towards the ultimate conservation scheme: V. A second order sequel to Godunov'f method', *J. Comput. Phys.*, **32**, 101–136 (1979).
18. S. Chakravarthy and S. Osher, 'Computing with high resolution: upwind schemes for hyperbolic equations', *Lect. Notes Appl. Math.*, **22**, 57–86 (1985).
19. M. Putti, W. W.-G. Yeh and W. A. Mulder, 'A triangular finite volume approach with high-resolution upwind terms for the solution of groundwater transport equations', *Water Resources Res.*, **26**, 2865–2880 (1990).
20. G. Chavent and J. Jaffre, *Mathematical Models and Finite Elements for Reservoir Simulation*, North-Holland, Amsterdam, 1986.
21. J. Bear, *Hydraulics of Groundwater*, McGraw-Hill, New York, 1979.
22. V. Gowda, 'Discontinuous finite elements for nonlinear scalar conservation laws', *Thèse de Doctorat, Université Paris IX-Dauphine, 1988.*
23. V. Gowda and J. Jaffre, 'A discontinuous finite element method for scalar nonlinear conservation laws', *Rapport de Recherche INRIA*, 1993.
24. P. G. Ciarlet, *Introduction à l'Analyse Numérique Matricielle et à l'Optimisation*, Masson, Paris, 1988.
25. P. A. Raviart and J. M. Thomas, 'A mixed finite element method for the second order elliptic problems', *Mathematical Aspects of the Finite Element Method*, Springer, New York, 1977.
26. J. M. Thomas, 'Sur l'analyse numérique des méthodes d'éléments finis hybrides et mixtes', *Thèse de Doctorat d'Etat*, Université Pierre et Marie Curie, 1977.
27. G. Chavent and J. E. Roberts, 'A unified physical presentation of mixed, mixed hybrid finite elements and standard finite difference approximations for the determination of velocities in waterflow problems', *Adv. Water Resources*, **14**, 329–348 (1991).
28. J. Leij Feike and J. H. Dane, 'Analytical solution of the one-dimensional advection equation and two- or three-dimensional dispersion equation', *Water Resources Res.*, **26**, 1475–1482 (1990).
29. L. Kaddouri, 'Une méthode d'éléments finis discontinus pour les équations d'Euler des fluides compressibles', *Thè, Université Paris VI, 1993.*

